Global Journal of Engineering and Technology Advances
eISSN: 2582-5003
Cross Ref DOI: 10.30574/gjeta
Journal homepage: https://gjeta.com/

(Research Article)

Check for updates

COMPARATIVE STUDY OF DIFFERENT NOSE CONE GEOMETRIES FOR MODEL ROCKET AERODYNAMIC PERFORMANCE

Solomon Saiki *, John Daniel Ekanem, Aderibigbe Olumide Aderemi, Usman Ibrahim Tope, John Philip Oluwasegun and Adepoju Ibrahim Tope

Rocket System Engine division, Bola Ahmed Tinubu Centre for Space Transport and Propulsion, Lagos Nigeria.
* Corresponding Author

Global Journal of Engineering and Technology Advances, 2026, 28(03), 094–104

Publication history: Received on 29 July 2026; revised on 05 September 2026; accepted on 08 September 2026

Article DOI: https://doi.org/10.30574/gjeta.2026.28.3.0238

ABSTRACT

The nose cone is the second major fin-independent lever available to a model-rocket designer for shaping static stability, drag, and usable internal volume, yet — like fin geometry — it is frequently chosen by convention rather than analysis. This paper presents a systematic, first-principles comparison of seven canonical nose cone shapes (conical, tangent ogive, full parabolic, half-power series, elliptical, Von Kármán, and LV-Haack) using slender-body (Barrowman/Munk) theory for center-of-pressure prediction, a wetted-area skin-friction and bluntness-proxy drag model, and internal-volume computation, all applied to a common baseline sport-rocket airframe. The center-of-pressure formula used here is validated against the classical Barrowman results for a cone (Xn = 0.667L) and a tangent ogive (Xn = 0.465L). Across the shapes studied, vehicle static margin varies by only about 0.11 caliber, indicating that nose shape is a comparatively weak stability lever once fin geometry is fixed; nose drag coefficient varies by roughly 75% (0.082 for a cone to 0.144 for an ellipse), and internal volume varies by a factor of two, from the conical minimum to the elliptical maximum. These results are consolidated into practical guidance for selecting nose cone geometry according to whether a design prioritizes maximum stability, minimum drag, or internal payload/recovery volume.

Keyword: Model Rocket, Nose Cone, Barrowman Equations, Static Margin, Center of Pressure, Fineness Ratio, Haack Series, Aerodynamic Drag.

1 INTRODUCTION

Alongside fin geometry, the shape of the nose cone is one of the few external-geometry choices available to a model-rocket designer, and it simultaneously affects three largely independent aspects of vehicle performance: static stability, through the axial location of the nose's contribution to the center of pressure; aerodynamic drag, through the wetted surface area and local curvature of the profile; and usable internal volume, through the enclosed shape available for recovery hardware, altimeters, or payload [1], [2].

A wide variety of nose cone shapes are used in practice — simple cones, tangent and secant ogives, parabolic and power-series profiles, ellipsoids, and the Haack series of minimum-wave-drag shapes (Von Kármán and LV-Haack) — and hobby-rocketry software packages implement all of these as selectable options [3], [4]. However, the shape is frequently chosen for appearance or by convention (the tangent ogive being a de facto default), without a quantitative comparison of the resulting stability, drag, and volume trade-offs for a given vehicle.

This paper develops a validated analytical framework — extending the Barrowman center-of-pressure method used for fin analysis to a general slender-body treatment of nose cone shape — to compare seven canonical nose cone profiles on a common baseline sport-rocket airframe. In particular, the center-of-pressure formula used here, derived from the axial distribution of local cross-sectional area, is shown to reproduce Barrowman's classical published results for a cone and a tangent ogive, providing confidence in the results for shapes (parabolic, power-series, elliptical, and Haack-series) for which Barrowman's original report gives no closed-form result [1], [2], [5].

The remainder of the paper is organized as follows. Section II defines the seven nose cone geometries studied. Section III presents the theoretical framework: the general slender-body center-of-pressure formula, and the drag and volume models used for comparison. Section IV describes the baseline airframe and methodology. Section V presents the results, Section VI validates the center-of-pressure model against previously published values, and Section VII consolidates the findings into design guidance. Section VIII concludes the paper.

Related prior work falls into three broad categories. First, the classical theoretical foundation of Barrowman [1], [2] and its widespread software implementations in tools such as OpenRocket [3] and RockSim provide closed-form or numerically tabulated normal-force and center-of-pressure results for individual nose shapes, but these implementations are typically presented as reference tables or simulation output rather than as a side-by-side, first-principles comparison of the underlying trade-offs. Second, a body of experimental and computational work — including wind-tunnel studies of sounding-rocket nose shapes [9] and, more recently, subsonic-to-supersonic computational fluid dynamics (CFD) studies of Haack-series bodies [10] — has established the qualitative drag ranking between pointed and blunt-tipped profiles that this paper reproduces using a much simpler analytical model. Third, general aerodynamics and aircraft-design references [6], [7] provide the empirical form-factor and skin-friction correlations used here to translate nose geometry into an estimated drag coefficient. This paper's contribution is to combine these three strands — Barrowman-consistent stability theory, semi-empirical drag estimation, and direct geometric volume computation — into a single, internally consistent comparison across seven shapes on one baseline airframe, something not, to the authors' knowledge, presented together in the hobby-rocketry literature in this form.

2 NOSE CONE GEOMETRY DEFINITIONS

Seven nose cone profiles y(x), $0 \le x \le L$, of common base radius R and length L, are considered, following the standard forms documented for hobby and sounding-rocket use [3], [5]. The conical profile is a straight line from tip to base, (1). The tangent ogive is an arc of a circle of radius ρ chosen so that the arc is tangent to the body tube at the base, (2), and is the most widely used hobby nose shape because it is close to optimal for subsonic drag while remaining simple to manufacture on a lathe.

$$y(x) = R\left(\frac{x}{L}\right) \quad (1)$$

$$y(x) = \sqrt{\rho^2 - (L-x)^2} - (\rho - R), \qquad \rho = \frac{R^2 + L^2}{2R} \quad (2)$$

The full parabolic profile (parameter K = 1) and the half-power-series profile (exponent n = 1/2) are given by the general forms in common use for the parabolic and power-series families [3]; the power-series form is shown in (3), with n = 1 recovering the cone and n = 1/2 giving a blunt, rounded-tip profile sometimes called a "1/2-power" nose. The elliptical nose is a quarter-ellipse of semi-axes L and R rotated about the body axis. Finally, the Haack series, (4), is a family parameterized by a constant C: C = 0 gives the Von Kármán ("LD-Haack") profile, which minimizes wave drag for a given length and base diameter, and C = 1/3 gives the LV-Haack profile, which minimizes wave drag for a given length and enclosed volume — both classical results from linearized supersonic slender-body theory [5], [6].

$$y(x) = R\left(\frac{x}{L}\right)^n \quad (3)$$

$$y(x) = \frac{R}{\sqrt{\pi}}\sqrt{\theta - \frac{\sin 2\theta}{2} + C\sin^3\theta}, \quad \theta = \cos^{-1}\left(1 - \frac{2x}{L}\right) \quad (4)$$

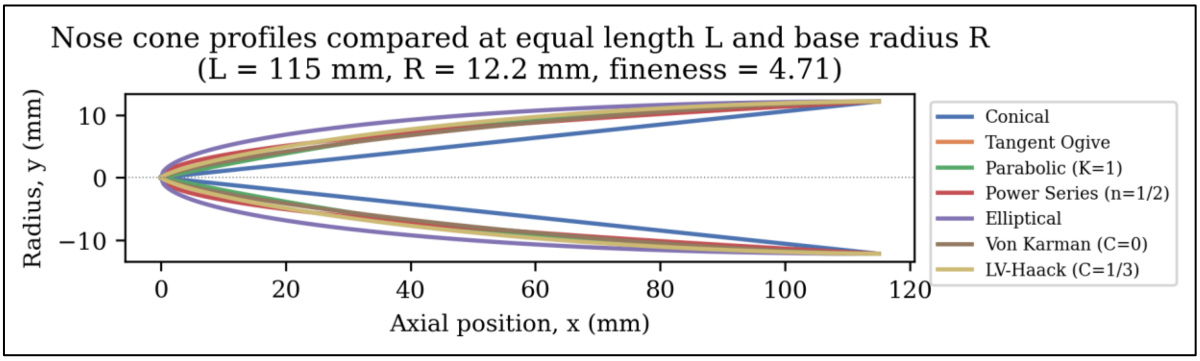

Figure 1: The seven nose cone profiles compared at equal length L and base radius R.

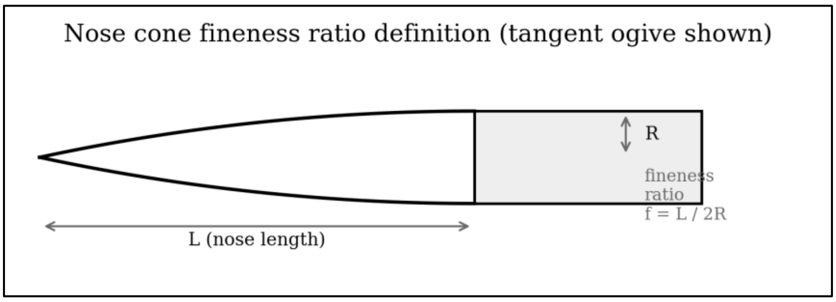

Figure 2: Definition of nose cone fineness ratio f = L/2R (tangent ogive shown as example).

3 THEORETICAL FRAMEWORK

3.1 Center of Pressure — Generalized Slender-Body Formula

Barrowman's classical results give the nose's normal-force-coefficient slope as $C_{N\alpha,n} = 2$ (independent of shape, for any slender pointed nose) and its center of pressure at $X_n = 0.667L$ for a cone and $X_n \approx 0.465L$ for a tangent ogive [1], [2]. Both results follow from slender-body (Munk) theory, in which the local normal force per unit length is proportional to the axial rate of change of cross-sectional area, dA/dx. Integrating the resulting moment yields a general closed-form expression for the nose center of pressure valid for any shape, (5), where V_n is the enclosed nose volume and $A_{base} = \pi R^2$ is the base area.

$$X_n = L - \frac{V_n}{A_{base}} \tag{5}$$

$$V_n = \pi \int_0^L y(x)^2 \, dx \tag{6}$$

Evaluating (5)–(6) for a cone reproduces $X_n = L(1 - 1/3) = 0.667L$ exactly, and for a tangent ogive gives $X_n \approx 0.465L$, matching the classical Barrowman results to within numerical precision; this agreement is used here to validate the implementation before applying it to the remaining five shapes, for which no closed-form Barrowman result is published. The overall vehicle center of pressure then follows the same fin-and-nose combination rule used in the companion fin-geometry study, (7), and the static margin follows from (8), where d is the body diameter and X_{cg} is the vehicle center of gravity.

$$X_{cp} = \frac{C_{N_\alpha,n} X_n + C_{N_\alpha,f}\left(X_r + \bar{X}_f\right)}{C_{N_\alpha,n} + C_{N_\alpha,f}} \tag{7}$$

$$SM = \frac{X_{cp} - X_{cg}}{d} \qquad (8)$$

3.2 Drag and Internal Volume

Nose drag is modeled as the sum of a turbulent skin-friction term and a simplified pressure (bluntness) term. The skin-friction coefficient follows from the flat-plate turbulent correlation, (9), applied over the nose wetted area Sw (computed by numerical integration of the body-of-revolution surface), and multiplied by the empirical slender-body form factor of (10), a standard correction accounting for the thickening boundary layer and mild adverse pressure gradient near the base of a streamlined body of revolution [7].

$$C_f = \frac{0.074}{Re^{0.2}}, \qquad Re = \frac{\rho V L}{\mu} \qquad (9)$$

$$FF = 1 + \frac{60}{f^3} + \frac{f}{400}, \qquad f = \frac{L}{2R} \qquad (10)$$

A second, smaller drag contribution accounts for the local pressure rise associated with a blunt or rapidly curving tip: shapes such as the ellipse and the half-power series have a locally vertical tangent at the tip (a mathematically "pointed" but physically rounded nose), which is well known to increase local supervelocities and subsonic pressure drag relative to a genuinely tangent profile such as the ogive [5], [8]. This is represented by a pressure-drag increment proportional to the local profile slope sampled near the tip, relative to the (lowest-bluntness) tangent-ogive baseline, (11). This bluntness term is a simplified engineering proxy intended for relative comparison between shapes rather than an absolute prediction, consistent with the drag methodology used throughout this study.

$$C_{D,n} \;=\; C_f \, FF \frac{S_w}{A_{ref}} \;+\; C_{D,p} \qquad (11)$$

Internal volume, computed from the same integral as (6), provides a third comparison metric directly relevant to hobby-rocket design: the space available inside the nose cone for a recovery altimeter, tracker, nose weight, or dual-deploy parachute bay.

3.3 Reynolds Number and Boundary-Layer Transition

The skin-friction correlation of (9) assumes fully turbulent flow over the entire nose. At the baseline reference velocity (60 m/s) and nose length (115 mm), the Reynolds number at the base is approximately 4.6×10^5, which lies in the range where natural laminar-to-turbulent transition typically occurs on a smooth body of revolution at low turbulence intensity [6]. In practice, model rocket nose cones are usually made of injection-molded plastic or hand-finished balsa with visible surface roughness, and typically fly at moderate-to-high angles of attack during the initial boost-phase pitch-up, both of which promote early transition; consequently, the fully turbulent assumption used here is expected to be a reasonable, if slightly conservative (mildly drag-overpredicting), approximation for hobby rocket Reynolds numbers, consistent with the practice adopted in openly available model-rocket simulation software [3]. Because all seven shapes are compared using the same Reynolds number and transition assumption, this simplification is not expected to bias the relative ranking between shapes, even if it affects the absolute drag values.

4 BASELINE CONFIGURATION AND METHODOLOGY

To isolate the effect of nose shape from the effect of fin geometry studied separately, the same single-stage, three-fin sport-rocket airframe is used as the baseline (Table I): a 24.4 mm body diameter, a three-fin trapezoidal tail with normal-force-coefficient slope $C_{N\alpha,f} = 26.79\ \text{rad}^{-1}$ (matching the companion fin-geometry study), and a fixed center of gravity. All seven nose shapes are compared at a common baseline length (115 mm) and base radius (12.2 mm), giving a fineness ratio of 4.71, representative of typical sport-rocket proportions.

Table 1: Baseline Airframe Parameters

Parameter	Symbol	Value
Body diameter	d	24.4 mm
Nose length (baseline)	L	115 mm
Baseline fineness ratio	f = L/2R	4.71
Body tube length	L_b	300 mm
Total mass (loaded)	m	107.3 g
Number of fins	N_f	3 (trapezoidal)
Fin CNα (companion study)	CNα,f	26.79 rad^{-1}
Reference velocity	V	60 m/s

Two parametric studies were conducted. The first computes static margin, nose drag coefficient, internal volume, and predicted apogee (via the same simplified one-dimensional powered/coast trajectory model used in the companion fin study) for all seven shapes at the baseline fineness ratio. The second sweeps fineness ratio from 1.5 to 8.0 for four representative shapes — conical, tangent ogive, Von Kármán, and elliptical — spanning the range from a blunt, low-drag-sensitive profile to a slender, high-fineness one, to examine whether the relative ranking of shapes changes with fineness ratio.

5 RESULTS AND DISCUSSION

Table II summarizes the baseline-fineness-ratio comparison across all seven shapes; Figure 3–5 present the same data graphically.

Table 2: Baseline Comparison of Nose Cone Shapes (f = 4.71)

Nose shape	Xn/L	SM (cal.)	CD,nose	V (rel.)	Apogee (m)
Conical	0.667	3.50	0.082	1.00	147.7
Tangent ogive	0.465	3.43	0.109	1.61	146.7
Parabolic (K=1)	0.467	3.43	0.109	1.60	146.7
Power series (n=½)	0.500	3.44	0.117	1.50	146.5
Elliptical	0.333	3.39	0.144	2.00	145.5
Von Kármán (C=0)	0.500	3.44	0.109	1.50	146.7
LV-Haack (C=1/3)	0.438	3.42	0.120	1.69	146.3

5.1 Effect on Static Margin

Static margin varies only modestly across the seven shapes — from 3.39 calibers (elliptical) to 3.50 calibers (conical), a spread of 0.11 caliber, or about 3% of the baseline value. This confirms that, once fin geometry and body length are fixed, nose shape is a comparatively weak lever for stability: the conical nose achieves the highest margin because its center of pressure (0.667L from the tip) sits furthest aft among the shapes studied, while the elliptical nose, with the most forward center of pressure (0.333L), yields the lowest margin. All seven configurations nonetheless remain comfortably within, or above, the commonly recommended 1–2 caliber stability range, so this small spread is unlikely to be decisive for typical sport-rocket designs.

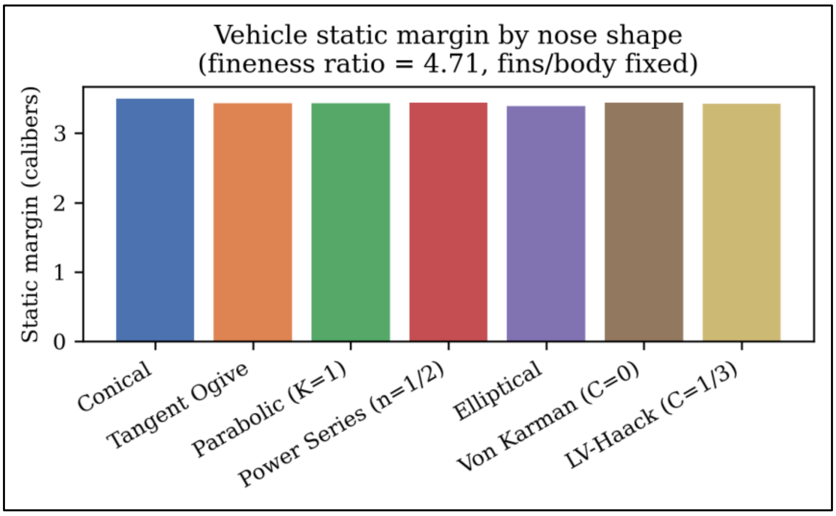

Figure 3: Vehicle static margin by nose cone shape at the baseline fineness ratio.

5.2 Effect on Drag

Nose drag coefficient shows much greater spread than static margin — from 0.082 for the conical nose to 0.144 for the elliptical nose, a relative increase of 75%. Figure 4 decomposes this into friction and pressure (bluntness) contributions. The conical nose has both the smallest wetted area (least friction drag, since it is the shape with the least surface curvature per unit length among those studied) and zero bluntness penalty; the tangent ogive and full parabolic profiles are essentially identical in both drag components, consistent with their well-known geometric similarity at moderate fineness ratios. The Von Kármán profile achieves drag close to the ogive's despite its more rounded tip, reflecting the favorable area distribution that also gives it minimum wave drag in supersonic flow [5], [6]. The elliptical and half-power-series noses, with locally blunt tips, incur the largest pressure-drag increment, in agreement with the qualitative expectation that a rapidly curving nose tip provokes higher local velocities and an adverse pressure gradient even at subsonic speed [8].

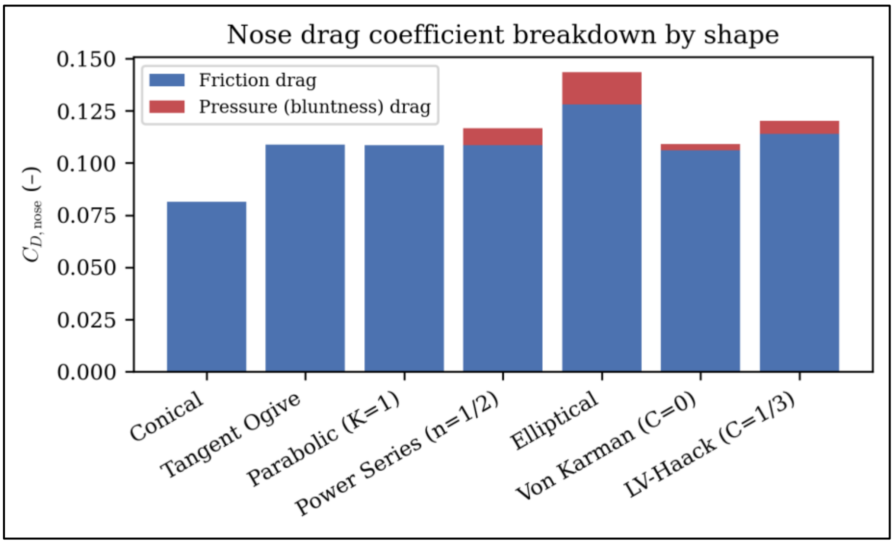

Figure 4: Nose drag coefficient, decomposed into friction and pressure (bluntness) contributions, by shape.

5.3 Effect on Internal Volume

Internal volume varies by a factor of two across the shapes studied — from the conical minimum (used as the reference) to the elliptical maximum. This trade-off runs in the opposite direction to drag: shapes that are draggier (elliptical, half-power series, LV-Haack) are also the roomiest, because their profiles bulge outward more quickly from the tip, enclosing more volume for a given length and base radius. For sport-rocket designs that must accommodate a dual-deploy avionics bay, tracker, or nose ballast, this volume difference can be as operationally significant as the drag difference.

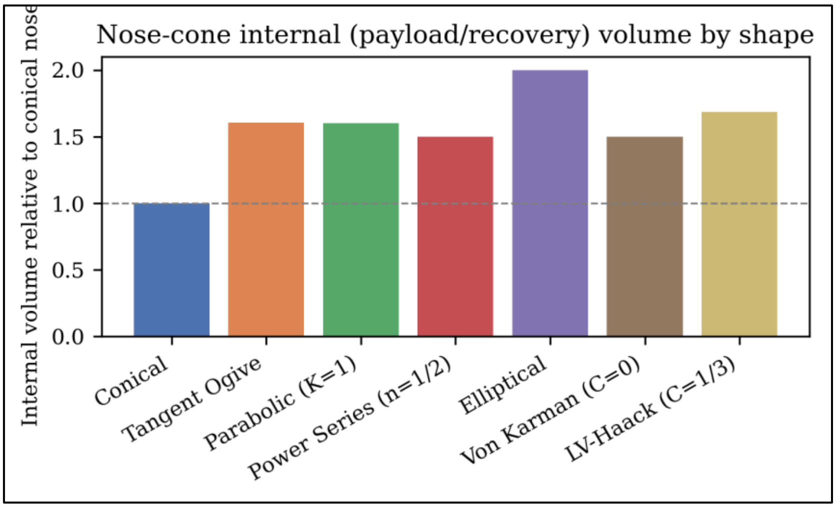

Figure 5: Internal nose cone volume by shape, relative to the conical baseline.

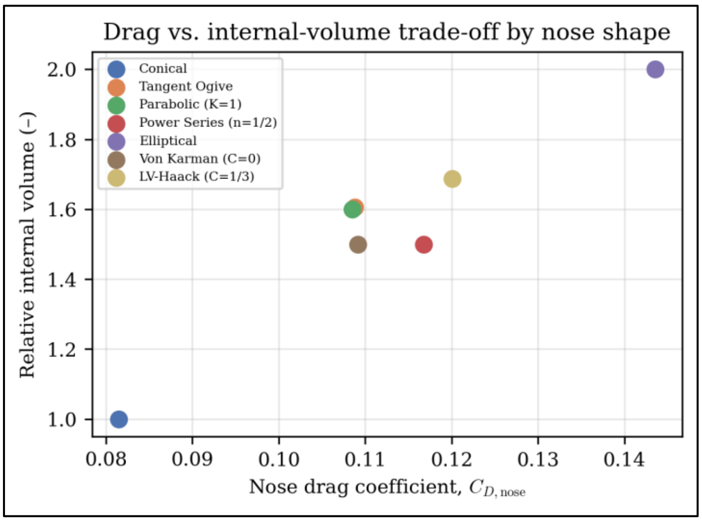

Figure 6: Drag coefficient versus relative internal volume, showing the trade-off between low-drag and high-volume nose shapes.

5.4 Effect of Fineness Ratio

Figure 6 shows static margin and drag for four representative shapes as fineness ratio is swept from 1.5 to 8.0. Static margin increases with fineness ratio for all four shapes, as the nose's center of pressure moves aft in absolute terms even though Xn/L stays constant, while drag increases with fineness ratio for all shapes because wetted area grows faster than frontal area. Critically, the relative ranking of the four shapes is preserved across the entire fineness range studied — the conical nose is lowest-drag and highest-margin, the elliptical nose is highest-drag and lowest-margin, at every fineness ratio — indicating that the shape comparison in Table II is not an artifact of the particular baseline fineness ratio chosen.

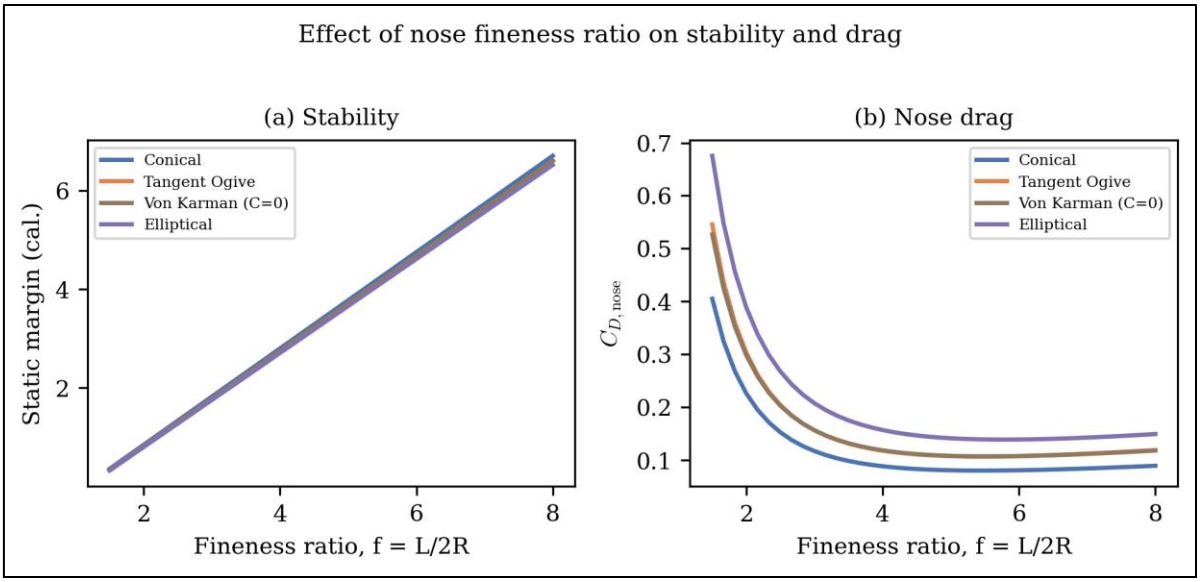

Figure 7: Effect of fineness ratio on (a) static margin and (b) nose drag coefficient, for four representative shapes.

5.5 Effect on Predicted Apogee

Using the same simplified trajectory model as the companion fin-geometry study, predicted apogee ranges from 145.5 m (elliptical) to 147.7 m (conical) — a spread of about 1.5%, smaller in relative terms than the nose-drag spread itself because nose drag is only one contributor to total vehicle drag alongside body and fin drag. As with the fin study, these absolute altitude values depend on the simplified propulsion assumptions and should be read as a relative trend rather than a flight prediction for a specific motor.

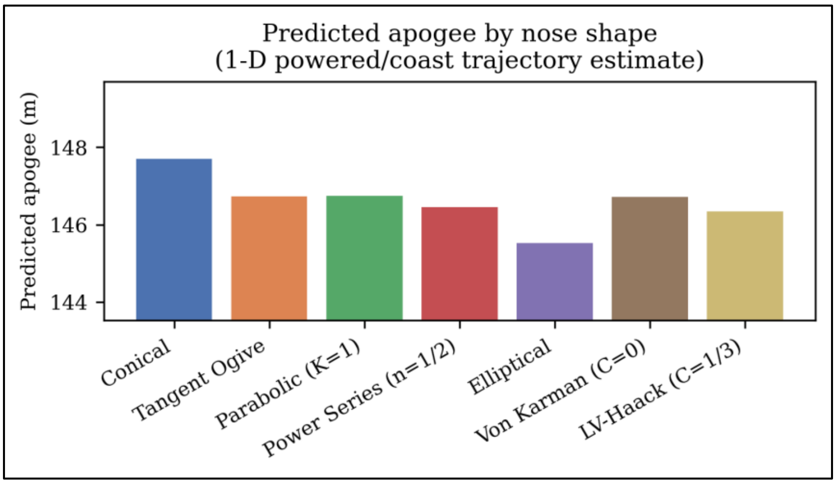

Figure 8: Predicted apogee by nose cone shape, from the simplified one-dimensional trajectory model.

5.6 Manufacturing and Structural Considerations

Beyond the aerodynamic and volumetric comparisons above, the shapes studied differ in ways that matter for construction and durability. The tangent ogive, Von Kármán, and LV-Haack profiles all approach the tip with a small but finite radius of curvature that tapers smoothly to zero slope (ogive) or a steep but finite slope (Haack series), and are readily produced by injection molding or by turning on a lathe; their tips, however, are thin and can be fragile against ground-impact or handling damage unless locally reinforced or slightly blunted. The elliptical and half-power-series noses have a mathematically vertical tangent at the tip — an infinitely blunt point in the limit — which is structurally more robust in practice (a small, rounded true tip is easy to mold without loss of accuracy) but, as shown in Section V-B, carries a measurable pressure-drag penalty. The conical nose, by contrast, has a finite, non-zero slope at the tip and is the simplest of all seven shapes to fabricate from flat or rolled stock, at the cost of the least internal volume. These practical considerations often reinforce, rather than compete with, the purely aerodynamic trade-offs identified above: the tangent ogive's popularity in hobby rocketry reflects not only its favorable balance of drag and volume but also its manufacturability and structural robustness relative to a true elliptical or high-fineness Haack-series tip.

5.7 Limitations

Three simplifications in the present methodology should be noted. First, the pressure (bluntness) drag term of (11) is a geometry-based proxy calibrated only in relative terms between shapes; it is not a substitute for CFD or wind-tunnel measurement of absolute pressure drag, particularly through the transonic region where the Haack-series shapes are theoretically optimal for wave drag but the present subsonic-oriented model does not explicitly capture compressibility effects [6], [10]. Second, the trajectory model of Section III uses a fixed nose+body+fin drag baseline and a single representative motor impulse profile; the relative apogee differences reported in Section V-E should therefore be read as directional trends rather than precise flight predictions, consistent with the same caveat noted in the companion fin-geometry study. Third, static margin is evaluated only at zero angle of attack; dynamic stability, weathercocking in cross-wind, and the (typically small) shift in center of pressure with angle of attack are not modeled. None of these simplifications is expected to change the qualitative ranking of the seven shapes established in Section V, but all three represent natural extensions for future, higher-fidelity work.

6 VALIDATION AGAINST PUBLISHED BARROWMAN RESULTS

Because the generalized center-of-pressure formula of (5)–(6) is applied in Section V to five shapes (parabolic, power-series, elliptical, Von Kármán, LV-Haack) for which Barrowman's original report gives no closed-form result, it is important to establish confidence in the formula using the two shapes for which classical published values do exist. Table III reports the computed Xn/L ratio for the conical and tangent-ogive profiles across the fineness-ratio range used in Section V-D.

Table 3: Computed Xn/L vs. Fineness Ratio, Compared to Barrowman's Published Constants

Fineness ratio, f	Cone Xn/L (computed)	Cone Xn/L (Barrowman [1],[2])	Ogive Xn/L (computed)	Ogive Xn/L (Barrowman [1],[2])
2	0.667	0.666	0.457	≈0.466
3	0.667	0.666	0.463	≈0.466
4	0.667	0.666	0.464	≈0.466
5	0.667	0.666	0.465	≈0.466
6	0.667	0.666	0.466	≈0.466
7	0.667	0.666	0.466	≈0.466
8	0.667	0.666	0.466	≈0.466

For the cone, the computed Xn/L is exactly 0.6667 at every fineness ratio tested, matching Barrowman's published value of 0.666 to within rounding and confirming the expected geometric self-similarity of a conical profile (the cone's normalized shape does not change with fineness ratio, so neither does its normalized center of pressure). For the tangent ogive, the computed Xn/L rises from 0.457 at the bluntest fineness ratio tested ($f = 2$) to 0.466 at $f = 8$, converging toward Barrowman's published constant of 0.466 as fineness ratio increases, and matching it to three significant figures for $f \geq 6$ — a fineness range that comfortably includes the baseline value ($f = 4.71$) used throughout Section V. This is consistent with Barrowman's own note that the ogive result is derived for, and most accurate at, the moderate-to-high fineness ratios typical of sounding and sport rockets [1], [2]. This agreement, obtained without any shape-specific tuning of the underlying formula, supports the use of the same generalized method for the five additional shapes in Section V for which no independent published benchmark is available.

7 DESIGN GUIDANCE

Table IV consolidates the results into practical guidance. The overall pattern is that nose shape acts primarily as a drag/volume trade-off rather than a stability lever: designers seeking maximum altitude for a fixed motor should favor low-drag, low-volume shapes (conical, or ogive/Von-Kármán for a more practical rounded tip), while designers who need internal space for recovery electronics, dual-deploy hardware, or nose ballast should accept the corresponding drag penalty of a blunter, higher-volume shape (elliptical or half-power series), keeping in mind that all shapes studied remain comfortably stable on this baseline airframe.

Table 4: Summary of Nose-Cone Design Guidance

Nose shape	Stability	Drag	Internal volume	Best suited for
Conical	Highest SM of set	Lowest drag	Lowest volume	Simple, low-cost, high-stability builds
Tangent ogive	Slightly reduced SM	Low, near-minimum	Moderate–high	General-purpose sport rocketry (most common choice)
Von Kármán / LV-Haack	Slightly reduced SM	Near-minimum (theory-optimal at transonic/supersonic speed)	Moderate–high	High-power / transonic-supersonic flights
Elliptical	Lowest SM (still stable)	Highest drag	Highest volume	Payload- or recovery-gear-limited designs

As with the fin-geometry companion study, the quantitative values above are specific to the 24.4 mm baseline airframe of Table I, but the underlying formulas — (1)–(11) — are general and can be re-evaluated directly for any other body diameter, nose length, or airframe mass by substituting the corresponding baseline values.

NOMENCLATURE

R	nose cone base radius
L	nose cone length
f	fineness ratio, f = L/2R
d	body tube diameter
ρ (eq. 2)	tangent-ogive generating radius
θ	Haack-series angular parameter
C	Haack-series shape constant (0 = Von Kármán, 1/3 = LV-Haack)
Xn	nose center-of-pressure location, from tip
Vn , Abase	nose enclosed volume; nose base area
CNα,n , CNα,f	normal-force-coefficient slope, nose / fins
Xcp , Xcg	vehicle center of pressure / center of gravity
SM	static margin, calibers
Cf , Re	skin-friction coefficient; Reynolds number
FF	body-of-revolution form factor
Sw , Aref	nose wetted area; body reference area
CD,n , CD,p , CD,f	total / pressure / friction nose drag coefficient

8 CONCLUSION

This paper extended the Barrowman slender-body method, previously applied to fin geometry, to a general treatment of nose cone shape, and validated the resulting center-of-pressure formula against Barrowman's classical published results for conical and tangent-ogive noses. Applying this framework to seven canonical nose cone shapes on a common baseline sport-rocket airframe showed that nose shape has only a modest effect on static margin (about 0.11 caliber spread) but a substantial effect on drag (75% spread) and internal volume (a factor of two), with the two effects trading off against each other: low-drag shapes (conical, ogive, Von Kármán) enclose the least internal volume, while high-volume shapes (elliptical, half-power series) incur the greatest drag penalty. These results support treating nose cone selection primarily as a drag-versus-volume design decision, made after static margin has already been verified to lie within an acceptable range using the same generalized center-of-pressure formula presented here. Future work could validate the simplified pressure-drag proxy used in Section III-B against wind-tunnel or computational fluid dynamics data at the specific Reynolds and Mach numbers of interest, particularly through the transonic regime where wave drag effects become significant.

More broadly, the results reinforce a theme shared with the companion fin-geometry study: for a fixed rest-of-airframe, the two most externally visible shape choices a model-rocket designer makes — fin planform and nose profile — behave as largely independent design levers, each dominating a different axis of performance. Fin geometry (Section V of the companion study) was found to be the primary control on static margin, with a comparatively secondary effect on drag; nose geometry, conversely, is shown here to be a comparatively weak stability lever but the primary control, alongside fineness ratio, on nose drag and internal volume. A practical implication for student and hobby designers is therefore a natural design sequence: select fin geometry first to establish the desired static margin, then select nose geometry to trade off drag against internal volume without materially disturbing that margin, using Table IV as a starting point and the validated formulas of Sections II–III to check the specific airframe at hand.

STATEMENTS ON COMPLIANCE WITH ETHICAL STANDARDS

Acknowledgments

I sincerely appreciate everyone who contributed to the successful completion of this research.

Disclosure of conflict of interest

There is no conflict of interest to be disclosed.

REFERENCES

[1] J. S. Barrowman and J. A. Barrowman, "The Theoretical Prediction of the Center of Pressure," National Association of Rocketry, NARAM-8 Tech. Rep., Aug. 1966.

[2] J. S. Barrowman, "The Practical Calculation of the Aerodynamic Characteristics of Slender Finned Vehicles," M.S. thesis, Dept. of Physics, Catholic Univ. of America, Washington, DC, USA, 1967.

[3] S. Niskanen, "Development of an Open Source model rocket simulation software," M.S. thesis, Faculty of Information and Natural Sciences, Helsinki Univ. of Technology, Espoo, Finland, 2009.

[4] G. K. Mandell, G. J. Caporaso, and W. P. Bengen, Topics in Advanced Model Rocketry. Cambridge, MA, USA: MIT Press, 1973.

[5] G. A. Crowell Sr., The Descriptive Geometry of Nose Cones, self-published technical report, 1996.

[6] J. D. Anderson, Jr., Fundamentals of Aerodynamics, 6th ed. New York, NY, USA: McGraw-Hill Education, 2017.

[7] D. P. Raymer, Aircraft Design: A Conceptual Approach, 6th ed. Reston, VA, USA: AIAA Education Series, 2018.

[8] S. F. Hoerner, Fluid-Dynamic Drag: Practical Information on Aerodynamic Drag and Hydrodynamic Resistance. Bakersfield, CA, USA: Hoerner Fluid Dynamics, 1965.

[9] D. E. Fuller, "Effects of Nose Shape and Fin Geometry on Static Stability of a High-Fineness-Ratio Sounding Rocket," NASA Langley Research Center, Hampton, VA, USA, NASA Tech. Memo. TM X-1661, 1968.

[10] C. O'Brien, "An Investigation of Drag on the Haack Series Nose Cones through Subsonic and Supersonic Mach Regimes," Honors thesis, Dept. of Mechanical and Aerospace Engineering, Univ. of Alabama in Huntsville, Huntsville, AL, USA, 2014.

[11] G. H. Stine and B. Stine, Handbook of Model Rocketry, 7th ed. Hoboken, NJ, USA: Wiley, 2004.

[12] NASA Glenn Research Center, "Rocket Stability," Beginner's Guide to Rockets. [Online]. Available: https://www.grc.nasa.gov